In vivo demonstration of photoacoustic-guided liver surgery

Kelley M. Kempski, Alycen Wiacek, Jasmin Palmer, Michelle Graham, Eduardo González, et al.

Kelley M. Kempski, Alycen Wiacek, Jasmin Palmer, Michelle Graham, Eduardo González, Bria Goodson, Derek Allman, Huayu Hou, Sarah Beck, Jin He, Muyinatu A. Lediju Bell, "In vivo demonstration of photoacoustic-guided liver surgery," Proc. SPIE 10878, Photons Plus Ultrasound: Imaging and Sensing 2019, 108782T (27 February 2019); doi: 10.1117/12.2510500

SPIE.

Event: SPIE BiOS, 2019, San Francisco, California, United States

In Vivo Demonstration of Photoacoustic-Guided Liver Surgery

Kelley M. Kempski[a], Alycen Wiacek[b], Jasmin Palmer[c], Michelle Graham[b], Eduardo González[d], Bria Goodson[e], Derek Allman[b], Huayu Hou[b], Sarah Beck[f], Jin He[g,h], and Muyinatu A. Lediju Bell[b,d]

[a]Department of Biomedical Engineering, University of Delaware, Newark, DE
[b]Department of Electrical & Computer Engineering, Johns Hopkins University, Baltimore, MD
[c]Department of Mechanical Engineering, Massachusetts Institute of Technology, Cambridge, MA
[d]Department of Biomedical Engineering, Johns Hopkins University, Baltimore, MD
[e]Department of Biology, Delta State University, Cleveland, MS
[f]Department of Molecular & Comparative Pathobiology, Johns Hopkins Medicine, Baltimore, MD
[g]Department of Surgery, Johns Hopkins Medicine, Baltimore, MD
[h]Department of Oncology, Johns Hopkins Medicine, Baltimore, MD

ABSTRACT

Liver surgeries carry considerable risk of injury to major blood vessels, which can lead to hemorrhaging and possibly patient death. Photoacoustic imaging is one solution to enable intraoperative visualization of blood vessels, which has the potential to reduce the risk of accidental injury to these blood vessels during surgery. This paper presents our initial results of a feasibility study, performed during laparotomy procedures on two pigs, to determine *in vivo* vessel visibility for photoacoustic-guided liver surgery. Delay-and-sum beamforming and coherence-based beamforming were used to display photoacoustic images and differentiate the signal inside blood vessels from surrounding liver tissue. Color Doppler was used to confirm vessel locations. Results lend insight into the feasibility of photoacoustic-guided liver surgery when the ultrasound probe is fixed and the light source is used to interrogate the surgical workspace.

1. INTRODUCTION

Liver surgeries carry considerable risk of gastrointestinal and intraabdominal hemorrhage and death.[1,2] Morbidity and mortality occur in 23-46% and 4-5%, of liver resections, respectively.[3] Thus, there is a salient clinical need to visualize major hepatic blood vessels during surgery to reduce the risk of vascular injury. To address this need, one of the most promising image guidance options is ultrasound imaging because it provides portable, real-time, multiplanar views at low cost. However, there are two limitations with ultrasound-based options. First, while color Doppler imaging can provide an ultrasound-based map of blood flow, it does not provide information about the location of a surgical tool relative to blood vessels. Second, although traditional ultrasound imaging can provide information with a color Doppler image overlay, metal surgical tools tend to produce reverberation artifacts that confound the ultrasound images, which are further degraded when acoustic clutter is present.[4,5]

Photoacoustic imaging is a relatively new imaging modality which uses a laser to irradiate a target to produce acoustic pressure waves that can be recorded by an ultrasound probe.[6] When paired with traditional ultrasound imaging, photoacoustic images have improved sensitivity and specificity with clearer tissue boundaries.[7] Due to the high optical absorption of metal,[8] a surgeon can simultaneously view a surgical tool tip and the blood vessel in the same photoacoustic-ultrasound coupled image,[9] which makes this an attractive imaging technique to guide surgery. The feasibility of photoacoustic-guided surgery has been explored for multiple surgeries and procedures, including spinal fusion surgeries,[10] fetal surgeries,[11] neurosurgeries,[12] and hysterectomies.[13,14] In particular, our lab is developing new light delivery systems that attach to surgical tools, with the ultrasound

Photons Plus Ultrasound: Imaging and Sensing 2019, edited by Alexander A. Oraevsky, Lihong V. Wang,
Proc. of SPIE Vol. 10878, 108782T · © 2019 SPIE · CCC code: 1605-7422/19/$18 · doi: 10.1117/12.2510500

probe placed externally for photoacoustic guidance of minimally invasive surgical procedures performed with and without robotic assistance.[13–16]

While the potential for photoacoustic-guided liver surgery was previously investigated using phantoms,[17,18] *in vivo* vessel visualization is expected to be challenging because of the highly vascularized nature of liver tissue.[17,19] Bell et al.[20] visualized targets as deep as 3 cm in *ex vivo* liver tissue that contained a significant amount of retained blood. To achieve these images, light from a 1064 nm Nd:YAG laser was delivered through a 1 mm core diameter optical fiber surrounded by a light diffusing sheath.[20] Similarly, Mitcham et al.[18] achieved photoacoustic signals as deep as 7 cm with an interstitial light source inserted in *ex vivo* liver tissue.

To the authors' knowledge, no previous studies investigate the feasibility of interventional photoacoustic liver imaging *in vivo*, thus expectations regarding the performance of this imaging method during liver surgeries remains to be determined. This paper presents the results of our initial exploration of *in vivo* photoacoustic imaging of major hepatic vessels in a pig animal model.

2. METHODS

2.1 Experimental Procedure

All procedures were approved by the Johns Hopkins University Institutional Animal Care and Use Committee, and all experiments were conducted at the Johns Hopkins Minimally Invasive Surgical Training and Innovation Center. Two *Sus domesticus* crossbred domestic pigs (5 and 6 months, 65 and 90 lbs., 2 female) were obtained for this study. The pigs were anesthetized and subsequently intubated to provide gas anesthesia throughout the surgery. A midline incision exposed the abdominal organs.

The photoacoustic imaging system placed next to the operating table consisted of an Alpinion ECUBE 12R ultrasound system connected to an Alpinion L3-8 linear transducer (Alpinion, Seoul, Korea) and an OPOTEK Phocus Mobile laser (OPOTEK, Carlsbad, CA) connected to a 5 mm-diameter fiber bundle. A fixed laser wavelength of 750 nm was chosen to visualize blood vessels throughout the experiments. The ultrasound probe used to receive the photoacoustic signals was either held by a Sawyer robot (Rethink Robotics, Boston, MA) or by hand. The ultrasound system was also used to acquire co-registered ultrasound images and color Doppler images to confirm vessel locations.

An open laparotomy was performed to gain access to the liver, and photoacoustic imaging was used to identify the hepatic veins in the liver. Energies of 40.8 mJ and 40.0 mJ were used to excite the blood vessels. A 3-dimensional (3D) reconstruction of the hepatic vein was created with the robot-held ultrasound probe translating in 1 mm increments across the liver surface, pausing at each increment to acquire end-inspiration photoacoustic or color Doppler images.

Fluence was calculated from recorded energies, E, and the area of the incident light, as defined by $\Phi = \frac{E}{\pi r^2}$: where r represents the radius of the 5 mm-diameter fiber bundle. We assume that the light source was placed in direct contact with the tissue, thus these calculations represent a conservative estimate of fluence.

2.2 Data Analysis

Photoacoustic images were created using delay-and-sum (DAS) beamforming and short-lag spatial coherence (SLSC) beamforming.[20,21] SLSC beamforming displays the spatial coherence of backscattered pressure waves by first finding the normalized spatial correlation between equally spaced elements, or lags, over an axial kernel $k = n_1 - n_2$ equivalent to one wavelength. The normalized spatial correlation is defined as:

$$\hat{\mathrm{R}}(\mathrm{m}) = \frac{1}{N-m} \sum_{i=1}^{N-m} \frac{\sum_{n=n_1}^{n_2} s_i(n) s_{i+m}(n)}{\sqrt{\sum_{n=n_1}^{n_2} s_i^2(n) \sum_{n=n_1}^{n_2} s_{i+m}^2(n)}} \tag{1}$$

where m is the lag, or the distance between two elements of the receive aperture in units of number of elements, N is the number of elements in the receive aperture, $s_i(\mathrm{n})$ is the time-delayed, zero-mean signal received by the ith element, and n is the sample depth in units of samples. The normalized spatial correlation, $\hat{R}$, is then

summed up to a specific short-lag value, M, resulting in the SLSC pixel value. This summation is performed for every axial and lateral position in the image. All SLSC images displayed are shown with $M = 5$, which corresponds to 7.8% of the number of elements in the receive aperture.

3. RESULTS

3.1 *In vivo* Liver Imaging

Fig. 1A shows the ultrasound image of an *in vivo* hepatic vein and a co-registered photoacoustic image created with DAS beamforming overlaid on this ultrasound image. The laser energy and corresponding fluence used to create the photoacoustic image were 40.8 mJ and 207.8 mJ/cm^2, respectively. The photoacoustic SLSC image created with the same channel data used to create the DAS image is shown in Fig. 1B. This SLSC image is overlaid on the ultrasound image in Fig. 1C and has the potential to minimize incoherent signals and artifacts associated with tissue surrounding the blood vessel. The color Doppler image confirming the location of the blood vessel in the liver is shown in Fig. 1D.

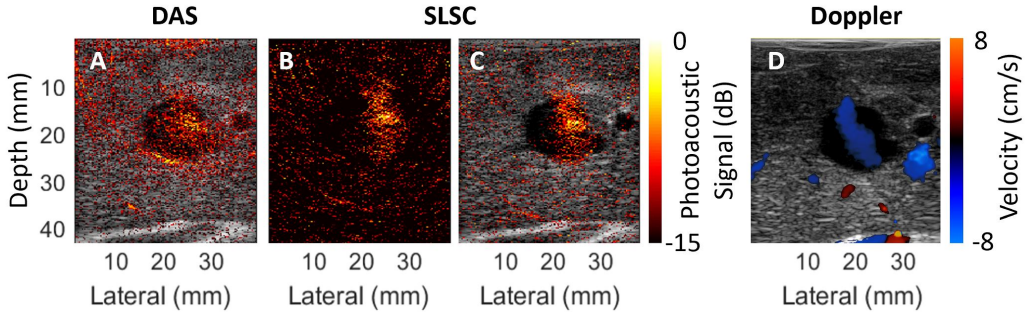

Figure 1. (A) DAS beamformed photoacoustic image of signals in *in vivo* liver overlaid on co-registered US image. (B) Corresponding SLSC beamformed photoacoustic image created with the same channel data. (C) SLSC beamformed photoacoustic image overlaid on US image. The photoacoustic images were acquired with 40.8 mJ energy. (D) Color Doppler confirmation of blood flow in the hepatic vein.

3.2 3D Vessel Imaging

Fig. 2 shows multiple display formats for the 3D vessel image data that was acquired with robotic assistance. The top row of Fig. 2 displays results associated with the photoacoustic signal, while the bottom row displays results associated with the color Doppler signal, which was used for confirmation of blood flow. The laser energy and corresponding fluence used to create the photoacoustic image were 40.0 mJ and 203.7 mJ/cm^2, respectively.

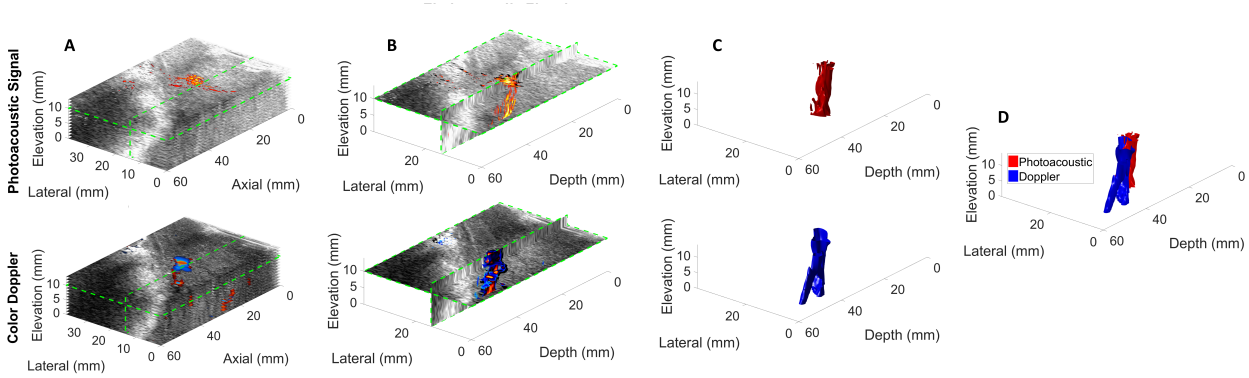

Figure 2. 3D representations of the hepatic vein created from photoacoustic and Color Doppler images. (A) Volume stack of photoacoustic and Doppler images acquired with Sawyer robot translating in 1 mm increments. (B) Biplanar cross section through the volume stack. (C) 3D reconstruction of hepatic vein segmented from photoacoustic and Doppler images. (D) Segmented vessels from photoacoustic and Doppler images combined with a different color for each imaging mode to show similarities between the two segmented vessel structures.

Fig. 2A shows the 3D stack of images used to form the volumetric data. Biplanar views of intersecting elevational and lateral slices are shown in Fig. 2B, with the chosen slices outlined in green in Fig. 2A. An isosurface of the segmented vessels based on the photoacoustic and Doppler volumetric image data is displayed in Fig. 2C.

Fig. 2D shows the two segmented vessels of Fig. 2C overlaid in the same spatial coordinate system. Differences in the image acquisition procedure likely contribute to the observed differences between the two segmented vessels. In particular, photoacoustic images were acquired as the robot stepped forward across the liver surface, while Doppler images were acquired as the robot retraced its steps in the opposite direction. Considering these two different motion directions, it is possible that the tissue deformed differently during the acquisition of each volume, which caused the vessels to be shifted relative to each other in Fig. 2D.

4. DISCUSSION

We successfully visualized *in vivo* hepatic veins within the liver. This success has two immediate implications for photoacoustic-guided liver surgeries. First, the visualization of major blood vessels during liver surgery can possibly help to improve navigation around these vessels during tissue resection procedures. The second implication is that this approach can be used to assist with estimating areas where cauterization of major blood vessels is necessary in order to mitigate bleeding and blood loss during surgery.

One perceived limitation of this approach could be the size and shape differences between the photoacoustic and Doppler images in Figs. 1 and 2. However, this perceived limitation can be explained by the photoacoustic signal only being present near the location of the 5 mm-diameter light source. This relatively small light source is unable to simultaneously illuminate all regions containing the blood signals. The capability to confidently limit the field of view (FOV) to a specific region of interest at the surgical site is one of the main advantages of using photoacoustic imaging to guide surgeries, as the presence of a major blood vessel near the surgical region of interest can be highlighted. In contrast, the Doppler images display all regions with blood flow. Although limiting the FOV may be possible with Doppler imaging, doing so would require the coordination of tool tip identification and knob adjustment on the ultrasound scanner during a surgical procedure.

The presented results are promising because they demonstrate that it is possible to obtain signals from *in vivo* blood vessels in the liver. Our future work will explore the minimum energy required to visualize these blood vessels and investigate signal appearance as a function of laser energy.

5. CONCLUSION

This work is the first to demonstrate *in vivo* blood vessel visualization with possible applications to a range of photoacoustic-guided liver surgeries. These findings are promising for surgical guidance when the ultrasound receiver is fixed and the light source is used to interrogate the surgical workspace.

Acknowledgments

This work was supported by NSF CAREER Award #1751522, REU Supplement to NSF CAREER Award #1751522, and the Computational Sensing & Medical Robotics Research Experience for Undergraduates program at Johns Hopkins University. The authors thank Nicholas Louloudis, Sue Eller, Ivan George, Dr. Lingdi Yin, and Dr. Liang Wang for animal care and surgery support and the Carnegie Center for Surgical Innovation. We also acknowledge the support of NVIDIA Corporation with the donation of the Titan Xp GPU that was used for portions of the signal processing required to display images presented in this paper.

REFERENCES

1. G. Rajarathinam, D. G. Kannan, V. Vimalraj, A. Amudhan, S. Rajendran, D. Jyotibasu, T. G. Balachandar, S. Jeswanth, P. Ravichandran, and R. Surendran, "Post Pancreaticoduodenectomy Haemorrhage: Outcome Prediction Based on New ISGPS Clinical Severity Grading.," *HPB : the official journal of the International Hepato Pancreato Biliary Association* **10**(5), pp. 363–70, 2008.

2. M. N. Wente, J. A. Veit, C. Bassi, C. Dervenis, A. Fingerhut, D. J. Gouma, J. R. Izbicki, J. P. Neoptolemos, R. T. Padbury, M. G. Sarr, C. J. Yeo, and M. W. Büchler, "Postpancreatectomy Hemorrhage (PPH)An International Study Group of Pancreatic Surgery (ISGPS) Definition," *Surgery* **142**, pp. 20–25, 7 2007.
3. F. Romano, M. Garancini, F. Uggeri, L. Degrate, L. Nespoli, L. Gianotti, A. Nespoli, and F. Uggeri, "Bleeding in Hepatic Surgery: Sorting through Methods to Prevent It.," *HPB Surgery : A World Journal of Hepatic, Pancreatic and Biliary Surgery* **2012**, p. 169351, 11 2012.
4. J. Huang, J. K. Triedman, N. V. Vasilyev, Y. Suematsu, R. O. Cleveland, and P. E. Dupont, "Imaging Artifacts of Medical Instruments in Ultrasound-Guided Interventions," tech. rep., 2007.
5. M. A. Lediju, M. J. Pihl, J. J. Dahl, and G. E. Trahey, "Quantitative assessment of the magnitude, impact and spatial extent of ultrasonic clutter," *Ultrasonic Imaging* **30**(3), pp. 151–168, 2008.
6. M. Xu and L. V. Wang, "Photoacoustic imaging in biomedicine," *Review of Scientific Instruments* **77**(041101), pp. 1–22, 2006.
7. R. Bouchard, O. Sahin, and S. Emelianov, "Ultrasound-guided photoacoustic imaging: Current state and future development," *IEEE Transactions on Ultrasonics, Ferroelectrics, and Frequency Control* , 2014.
8. L. G. Schulz, "The Optical Constants of Silver, Gold, Copper, and Aluminum I The Absorption Coefficient k," *Journal of the Optical Society of America* **44**, p. 357, may 1954.
9. B. Eddins and M. A. L. Bell, "Design of a multifiber light delivery system for photoacoustic-guided surgery," *Journal of biomedical optics* **22**(4), p. 041011, 2017.
10. J. Shubert and M. A. L. Bell, "Photoacoustic imaging of a human vertebra: implications for guiding spinal fusion surgeries," *Physics in Medicine and Biology* , 2018.
11. W. Xia, E. Maneas, D. I. Nikitichev, C. A. Mosse, G. S. dos Santos, T. Vercauteren, A. L. David, J. Deprest, S. Ourselin, P. C. Beard, *et al.*, "Interventional photoacoustic imaging of the human placenta with ultrasonic tracking for minimally invasive fetal surgeries," in *International Conference on Medical Image Computing and Computer-Assisted Intervention*, pp. 371–378, Springer, 2015.
12. M. A. L. Bell, A. K. Ostrowski, K. Li, P. Kazanzides, and E. M. Boctor, "Localization of transcranial targets for photoacoustic-guided endonasal surgeries," *Photoacoustics* **3**(2), pp. 78–87, 2015.
13. M. Allard, J. Shubert, and M. A. L. Bell, "Feasibility of photoacoustic-guided teleoperated hysterectomies," *Journal of Medical Imaging* **5**(2), p. 021213, 2018.
14. M. Allard, J. Shubert, and M. A. L. Bell, "Technical Note: Feasibility of photoacoustic guided hysterectomies with the da Vinci robot," in *Medical Imaging 2018: Image-Guided Procedures, Robotic Interventions, and Modeling*, **10576**, p. 105760A, International Society for Optics and Photonics, 2018.
15. N. Gandhi, M. Allard, S. Kim, P. Kazanzides, and M. A. L. Bell, "Photoacoustic-based approach to surgical guidance performed with and without a da vinci robot," *Journal of Biomedical Optics* **22**(12), p. 121606, 2017.
16. M. A. L. Bell and J. Shubert, "Photoacoustic-based visual servoing of a needle tip," *Scientific reports* **8**(1), p. 15519, 2018.
17. E. R. Hill, W. Xia, D. I. Nikitichev, K. Gurusamy, P. C. Beard, D. J. Hawkes, B. R. Davidson, and A. E. Desjardins, "Interventional multi-spectral photoacoustic imaging in laparoscopic surgery," in *Photons Plus Ultrasound: Imaging and Sensing 2016*, **9708**, p. 97080B, International Society for Optics and Photonics, 2016.
18. T. Mitcham, K. Dextraze, H. Taghavi, M. Melancon, and R. Bouchard, "Photoacoustic imaging driven by an interstitial irradiation source," *Photoacoustics* **3**(2), pp. 45–54, 2015.
19. C.-T. Germer, A. Roggan, J. P. Ritz, C. Isbert, D. Albrecht, G. Mü, and H. J. Buhr, "Optical Properties of Native and Coagulated Human Liver Tissue and Liver Metastases in the Near Infrared Range," tech. rep., 1998.
20. M. A. Lediju Bell, N. Kuo, D. Y. Song, and E. M. Boctor, "Short-lag Spatial Coherence Beamforming of Photoacoustic Images for Enhanced Visualization of Prostate Brachytherapy Seeds.," *Biomedical Optics Express* **4**(10), pp. 1964–77, 2013.
21. M. A. Lediju, G. E. Trahey, B. C. Byram, and J. J. Dahl, "Short-lag spatial coherence of backscattered echoes: imaging characteristics," *IEEE Transactions on Ultrasonics, Ferroelectrics and Frequency Control* **58**, pp. 1377–1388, Jul 2011.